6-2000

A Theoretical Study of the Reaction of Ti+ with Ethane

Jerzy Moc
Wroclaw University

Dmitri G. Fedorov
Iowa State University

Mark S. Gordon
Iowa State University, mgordon@iastate.edu

A Theoretical Study of the Reaction of Ti+ with Ethane

Abstract
The doublet and quartet potential energy surfaces for the Ti++C2H6→TiC2H+4+H2 and Ti++C2H6→TiCH+2+CH4reactions are studied using density functional theory(DFT) with the B3LYP functional and *ab initio*coupled cluster CCSD(T) methods with high quality basis sets. Structures have been optimized at the DFT level and the minima connected to each transition state (TS) by following the intrinsic reaction coordinate (IRC). Relative energies are calculated both at the DFT and coupled-cluster levels of theory. The relevant parts of the potential energy surface, especially key transition states, are also studied using multireference wave functions with the final energetics obtained with multireference second-order perturbation theory.

Keywords
Density functional theory, Chemical reaction theory, Cluster formation reactions, Coupled cluster, Hydrogen reactions

Disciplines
Chemistry

Comments
The following article appeared in *Journal of Chemical Physics* 112 (2000): 10247,and may be found at doi:10.1063/1.481666.

A theoretical study of the reaction of Ti + with ethane

Jerzy Moc, Dmitri G. Fedorov, and Mark S. Gordon

Citation: The Journal of Chemical Physics **112**, 10247 (2000); doi: 10.1063/1.481666
View online: http://dx.doi.org/10.1063/1.481666
View Table of Contents: http://scitation.aip.org/content/aip/journal/jcp/112/23?ver=pdfcov
Published by the AIP Publishing

A theoretical study of the reaction of Ti^+ with ethane

Jerzy Moc
Faculty of Chemistry, Wroclaw University, F.Joliot-Curie 14, 50-383 Wroclaw, Poland

Dmitri G. Fedorov and Mark S. Gordon[a)]
Department of Chemistry, Iowa State University, Ames, Iowa 50011

(Received 20 December 1999; accepted 22 March 2000)

The doublet and quartet potential energy surfaces for the $Ti^+ + C_2H_6 \rightarrow TiC_2H_4^+ + H_2$ and $Ti^+ + C_2H_6 \rightarrow TiCH_2^+ + CH_4$ reactions are studied using density functional theory (DFT) with the B3LYP functional and *ab initio* coupled cluster CCSD(T) methods with high quality basis sets. Structures have been optimized at the DFT level and the minima connected to each transition state (TS) by following the intrinsic reaction coordinate (IRC). Relative energies are calculated both at the DFT and coupled-cluster levels of theory. The relevant parts of the potential energy surface, especially key transition states, are also studied using multireference wave functions with the final energetics obtained with multireference second-order perturbation theory. © *2000 American Institute of Physics.* [S0021-9606(00)30623-7]

I. INTRODUCTION

Experimental studies of gas-phase reactions of the first-row transition-metal cations with simple alkanes provide valuable insight into the mechanism and energetics of C–H and C–C bond activation.[1] Insertion of the metal into C–H and/or C–C bonds is common and eventually leads to the elimination of H_2 or small alkanes.[1] In particular, several studies of Ti^+ reacting with ethane in the gas phase were conducted during the last 15 years using various mass spectrometric and ion beam techniques.[2–6] In an early experiment by the Freiser group,[2] an ion cyclotron resonance (ICR) method was used. Under single-collision conditions, only the C–H insertion leading to the H_2 elimination products, $TiC_2H_4^+ + H_2$, was observed.[2] Weisshaar and co-workers[3] employed a flow tube reactor technique to study the gas-phase reaction of Ti^+ with C_2H_6. In the multiple-collision environment of the flow reactor containing He buffer gas, the primary products found by these researchers were the adduct ions $TiC_2H_6^+$ and elimination products $TiC_2H_4^+ + H_2$, with the product distribution at 300 K determined to be 0.55 and 0.45, respectively.[3] Tolbert and Beauchamp,[4] who used an ion beam method, observed at a relative kinetic energy of 0.5 eV (11.5 kcal/mol) both the major elimination products $TiC_2H_4^+ + H_2$ and minor double elimination products, $TiC_2H_2^+ + 2H_2$, with a product distribution of 0.96 and 0.04, respectively. Based on the Ti^+ reactions with partially deuterated ethane, CH_3CD_3, Tolbert and Beauchamp suggested a 1,2-elimination mechanism for the dehydrogenation.[4] In the experiment of Sunderlin and Armentrout,[5] a guided-ion beam tandem mass spectrometer was used to examine the $Ti^+ + C_2H_6$ reaction, with the applied kinetic energies ranging from thermal to several eV. Six products were observed by these workers, with the H_2 elimination products indicated to be dominant at low energies.[5] The most recent experimental study of the gas-phase reaction of Ti^+ with ethane at thermal energies was conducted by the Castleman group[6] using the flow tube reactor technique. Consistent with the findings of Weisshaar,[3] the primary products observed by Castleman[6] under multiple-collision conditions were the adduct ions $TiC_2H_6^+$ and elimination products $TiC_2H_4^+ + H_2$, followed by the minor double elimination products $TiC_2H_2^+ + 2H_2$, with the product distribution determined as 0.30, 0.66, and 0.04, respectively.

In the present theoretical study, density functional theory (DFT) and *ab initio* calculations were carried out for the $Ti^+ + C_2H_6 \rightarrow TiC_2H_4^+ + H_2$ and $Ti^+ + C_2H_6 \rightarrow TiCH_2^+ + CH_4$ elimination reactions. The details of the potential energy surfaces (PES) involved are elucidated and the following particular issues are addressed:

(1) What is the actual structure of the adduct ions observed[3,6] in the flow tube experiments?
(2) Why were only the H_2 elimination products observed at low energies,[2–6] whereas the CH_4 elimination products were not?
(3) Is the H_2 elimination reaction of 1,1- or 1,2-type?
(4) How important are spin-orbit effects on the $Ti^+ + C_2H_6$ reaction?

II. COMPUTATIONAL METHODS

Structures were optimized with density functional theory (DFT)[7,8] using the hybrid B3LYP[9–11] functional of the form $(1-A)F_X^{\text{Slater}} + AF_X^{\text{HF}} + BF_X^{\text{Becke}} + CF_C^{\text{LYP}} + (1-C)F_C^{\text{VWN}}$, where F_X^{Slater} is the Slater exchange, F_X^{HF} is the Hartree–Fock exchange, F_X^{Becke} is the gradient part of the exchange functional of Becke,[9,10] F_C^{LYP} is the correlation functional of Lee, Yang, and Parr,[12] F_C^{VWN} is the correlation functional of Vosko, Wilk, and Nusair,[13] and *A*, *B*, *C* are the coefficients determined by Becke[9,10] using a fit to experimental heats of formation. The DFT force constant matrix was calculated at each stationary point to confirm its character [minimum or transition state (TS)] as well as to evaluate zero-point vibra-

[a)]Author to whom correspondence should be addressed.

tional energy (ZPVE) corrections, which are included in all the relative energies. To verify each pair of intermediates connected by a TS, the DFT intrinsic reaction coordinate (IRC)[14,15] was determined.[15]

The DFT B3LYP calculations employed the all-electron valence triple-zeta plus polarization (TZVP) basis set. For Ti, this consists of the $[10s6p]$ contraction of the $(14s9p)$ primitive set developed by Wachters[16] combined with the $[3d]$ contraction of the $(6d)$ primitive set taken from Rappé *et al.*[17] Wachters' *sp* basis was modified by replacing the most diffuse *s* function with one spanning the 3*s*-4*s* region ($\alpha_s=0.209$) and by adding two sets of *p* functions ($\alpha_p=0.156$ and 0.0611).[18] For C, the TZVP basis is composed of Dunning's[19a] $[5s3p]$ contraction of Huzinaga's $(10s6p)$ primitive set,[19b] augmented by a set of *d* polarization functions ($\alpha_d=0.72$). Similarly, for H, the $[3s]$ basis derived[19a] from the $(5s)$ primitive set,[19b] and augmented by a set of *p* polarization functions ($\alpha_p=1.0$), was used as TZVP.

The DFT B3LYP relative energies[20] are compared with those determined by the coupled-cluster singles and doubles method including a perturbative estimate of triples [CCSD(T)].[21] The large basis set denoted 6-311 +G(2*d*,2*p*) in GAUSSIAN 94[20a] was used in the CCSD(T) calculations. For Ti, this basis consists of the $[9s5p3d]$ contraction of Wachters' $(14s9p5d)$ primitive set,[16] supplemented with one diffuse *s* ($\alpha_s=0.01$),[22a] two sets of diffuse *p* ($\alpha_p=0.1016$ and 0.0340),[16] and one set of diffuse *d* functions ($\alpha_d=0.072$)[22b] as well as two sets of *f* polarization functions ($\alpha_f=1.38$ and 0.345).[20a,22c]

The relevant parts of the potential energy surface (in particular, the key TS's) were studied with complete active space self-consistent field (CASSCF)[23] wave functions and the final energetics were obtained using multiconfigurational second-order quasidegenerate perturbation theory (MCQDPT2).[24] The active space always included all six valence 4*s*3*d* orbitals and the corresponding electrons on Ti and the relevant C–H or C–C bonds in the pairs of bonding/antibonding orbitals. The all-electron valence triple-zeta (TZV)[18] basis set augmented with one *f*-polarization function[23] for Ti (TZV+*f*) was employed for the CASSCF and MCQDPT2 calculations.

Since the quartet and doublet potential energy surfaces appear to cross, and this crossing can affect the kinetics dramatically, the nonadiabatic coupling potential at the crossing (spin-orbit coupling) was studied. The spin-orbit coupling (SOC) was calculated with the TZV+*f* basis set and full Pauli–Breit Hamiltonian[25] using GAMESS[26] (for CASSCF wave functions). Nonorthogonal orbitals were used throughout for the SOC calculations; that is, the active orbitals were optimized for each multiplicity separately, but common core orbitals were used for both.

Three slightly different approaches were taken to locate the crossing of the doublet and quartet surfaces: (1) Follow the doublet IRC and calculate quartet energies for the corresponding doublet geometries at the IRC points. (2) Follow the quartet IRC and calculate the doublet energies at these IRC points. (3) Average the internal coordinates for doublet and quartet IRC points near the crossing; then emulate the IRC by varying the C–H bond distance, which is broken along this path (the imaginary mode of the C–H insertion **TS1-2** is mostly along the separation of the two atoms), and calculate doublet and quartet energies. This is called the averaged IRC.

TABLE I. Relative energies (in kcal/mol) for the $Ti^+(^4F)$ and $Ti^+(^2F)$ terms.

Method	$Ti^+(^4F,3d^24s^1)$	$Ti^+(^2F,3d^24s^1)$
CCSD(T)	0.0	4.0
CASSCF	0.0	16.6
DFT B3LYP	0.0	14.3
MCQDPT2	0.0	13.6
Expt.[a]	0.0	13.2

[a]Reference 27; averaged over *J* states.

III. RESULTS AND DISCUSSION

A. Reactants and products

The ground state of Ti^+ is $^4F\,(4s^13d^2)$ and the lowest doublet state is $^2F\,(4s^13d^2)$, the latter lying 13.2 kcal/mol higher in energy than the former.[27] As Table I shows, the $^2F-{}^4F$ splitting obtained by the MCQDPT2 method based on the multiconfigurational CASSCF (3/6) wave function (three active electrons in six active orbitals) compares most favorably with experiment. The ^2F state of Ti^+ is a three-electron doublet state and is difficult to describe with single configurational methods due to near degeneracy effects. Nevertheless, the DFT B3LYP estimate of the $^2F-{}^4F$ splitting is within 1 kcal/mol of the experimental result.[28] On the other hand, the CCSD(T) splitting of 4.0 kcal/mol is unreasonably low due to an overestimation of the correlation energy for the ^2F state. In the following discussion, it is assumed that DFT energies are reliable, except near transition structures and surface crossings.

The optimized structure of the second reactant C_2H_6, as well as those corresponding to the dehydrogenation and demethanation products of C_2H_6 by Ti^+, $TiC_2H_4^+ + H_2$ and $TiCH_2^+ + CH_4$, respectively, are depicted in Fig. 1. As expected,[10b,30] DFT reproduces the geometrical parameters of C_2H_6, CH_4, and H_2 very well. For the H_2 elimination product, $TiC_2H_4^+$, DFT predicts the quartet ($^4B_1$) to be the ground state separated from the lowest doublet state ($^2A_1$) by 1.8 kcal/mol. The CCSD(T) order is reversed, with the $^2A_1$ ground state 0.2 kcal/mol below $^4B_1$. The MCQDPT2 method predicts the $^2A_1$ state to be lower than $^4B_1$ by 3.1 kcal/mol. Sodupe *et al.*,[31] using the modified coupled-pair functional (MCPF) method at their self-consistent field (SCF) optimized geometries, predicted a $^2A_1$ ground state for $TiC_2H_4^+$ 5.2 kcal/mol below the high-spin $^4B_1$ state. For the $^2A_1$ state, the DFT and CASSCF $TiC_2H_4^+$ structures [Fig. 1(b)] are similar to the SCF structure of Sodupe *et al.*,[31] with a relatively short $Ti^+–C_2H_4$ distance of 1.937 Å (DFT) and 2.007 Å (CASSCF), and a significant H bend angle of 26.4° (DFT) and 28.3° (CASSCF).[32] The corresponding values of Sodupe *et al.* are 2.03 Å and 24.5°. For the $^4B_1$ state, a major difference between the DFT prediction and those of CASSCF and SCF[31] is a much shorter $Ti^+–C_2H_4$ distance of 2.287 vs 2.700 and 2.82 Å, respectively. The DFT $^4B_1$ struc-

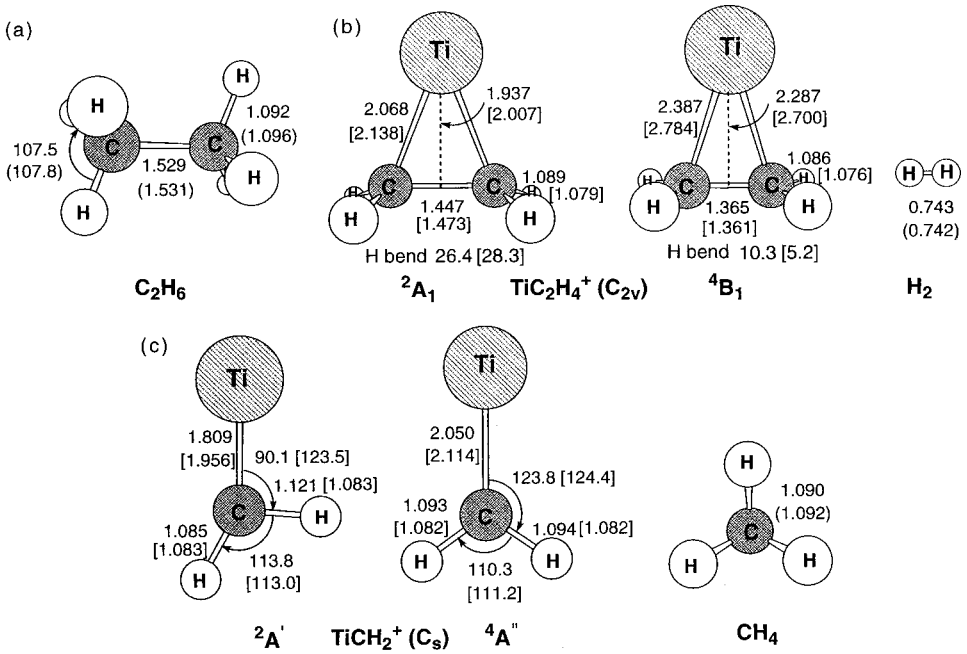

FIG. 1. Structure of (a) C_2H_6 reactant, (b) H_2 elimination products, and (c) CH_4 elimination products of C_2H_6 by Ti^+ (bond lengths in Å, bond angles in degrees). H bend denotes the out-of-plane bending angle of the hydrogen atoms (zero for the isolated C_2H_4). Values in parentheses are from experiment (taken from Ref. 29) and those in brackets are CASSCF results.

ture agrees with a coupled-cluster doubles (CCD)[21] geometry optimization that predicts 2.347 Å and 9.9° for the Ti^+–C_2H_4 distance and the H bend angle, respectively. Apparently, dynamic correlation implicit to some degree in DFT B3LYP and explicit in (CCD) markedly shortens the Ti^+–C_2H_4 interaction distance for the quartet state relative to the CASSCF and SCF results.

The CH_4 elimination product, $TiCH_2^+$, was studied previously at both *ab initio* and DFT levels.[33] The most recent DFT B3LYP calculations by Ricca and Bauschlicher[33a] revealed that the C_{2v} structure of $TiCH_2^+$ distorts to C_S as the latter symmetry allows donation from one of the C–H bonds to the empty Ti 3*d* orbital. The DFT B3LYP geometry of $TiCH_2^+$ in its lowest $^2A'$ state [Fig. 1(c)] agrees well with that of Ricca and Bauschlicher.[33a] Using the CASSCF wave function leads to the $TiCH_2^+$ ground-state doublet of C_{2v} symmetry. The CASSCF Ti–C distance of 1.956 Å and Ti–C–H angle of 123.5° for the doublet correspond favorably with the correlated modified coupled-pair functional (MCPF) results of 1.929 Å and 124.4°.[33c] The lowest quartet state of $TiCH_2^+$ [Fig. 1(c)] is found to lie 8.4 and 8.6 kcal/mol above the doublet according to DFT and CCSD(T), respectively. At the MCQDPT2 level of theory, the quartet state is 17.9 kcal/mol higher than the doublet.

B. Initial complexes

An ion-induced dipole complex $Ti^+\cdots C_2H_6$ has been proposed[3] as one candidate for the observed[3,6] $TiC_2H_6^+$ adduct ions. The computed structures for such complexes formed in the first step of the reaction between Ti^+ and C_2H_6 are denoted **1a** and **1b** in Fig. 2 and **1** in Figs. 3 (doublet) and 4 (quartet). Structure **1a** corresponds to an end-on approach of Ti^+ toward C_2H_6, while **1** and **1b** correspond to a side-on approach. Only C_s structures **1** and **1a** involving η^3 coordination appear to be minima on both surfaces, while η^2 coordinated structures **1b** with C_2 symmetry produced one imaginary frequency with the eigenvector clearly indicating distortion to **1**.[34] As Ti^+ has a quartet ground state, so have the initial complexes **1** and **1a** ($^4A''$). Complex **1** ($^4A''$) is bound by 20.1 and 15.6 kcal/mol relative to the $C_2H_6+Ti^+(^4F)$ reactants at the DFT B3LYP and CCSD(T) levels, respectively. The corresponding binding energies obtained for the complex **1a** are 18.7 and 14.9 kcal/mol, respectively. On the doublet surface, B3LYP complexes **1** and **1a** are bound by 20.5 and 20.1 kcal/mol with respect to $C_2H_6+Ti^+(^2F)$. As CCSD(T) breaks down for the doublet state of Ti^+, no reliable binding energies could be obtained

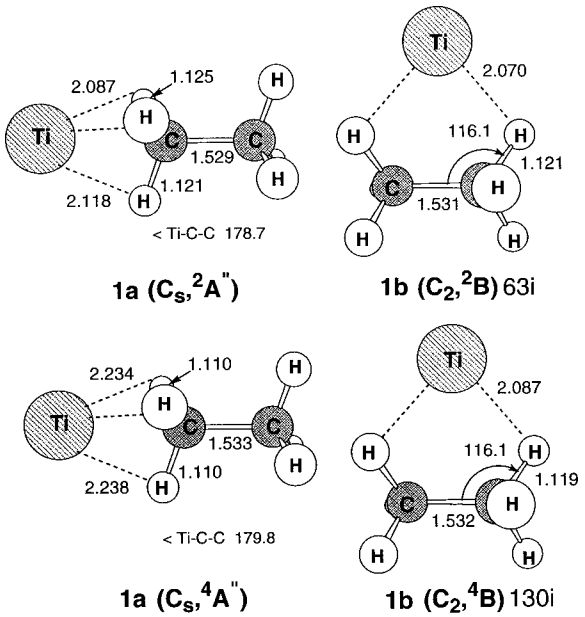

FIG. 2. Plausible structures of the ion-induced dipole complex $Ti^+\cdots C_2H_6$ formed in the first step of the reaction between Ti^+ and C_2H_6 (bond lengths in Å, bond angle in degrees); magnitudes of imaginary frequencies (cm^{-1}) for **1b** structures are shown.

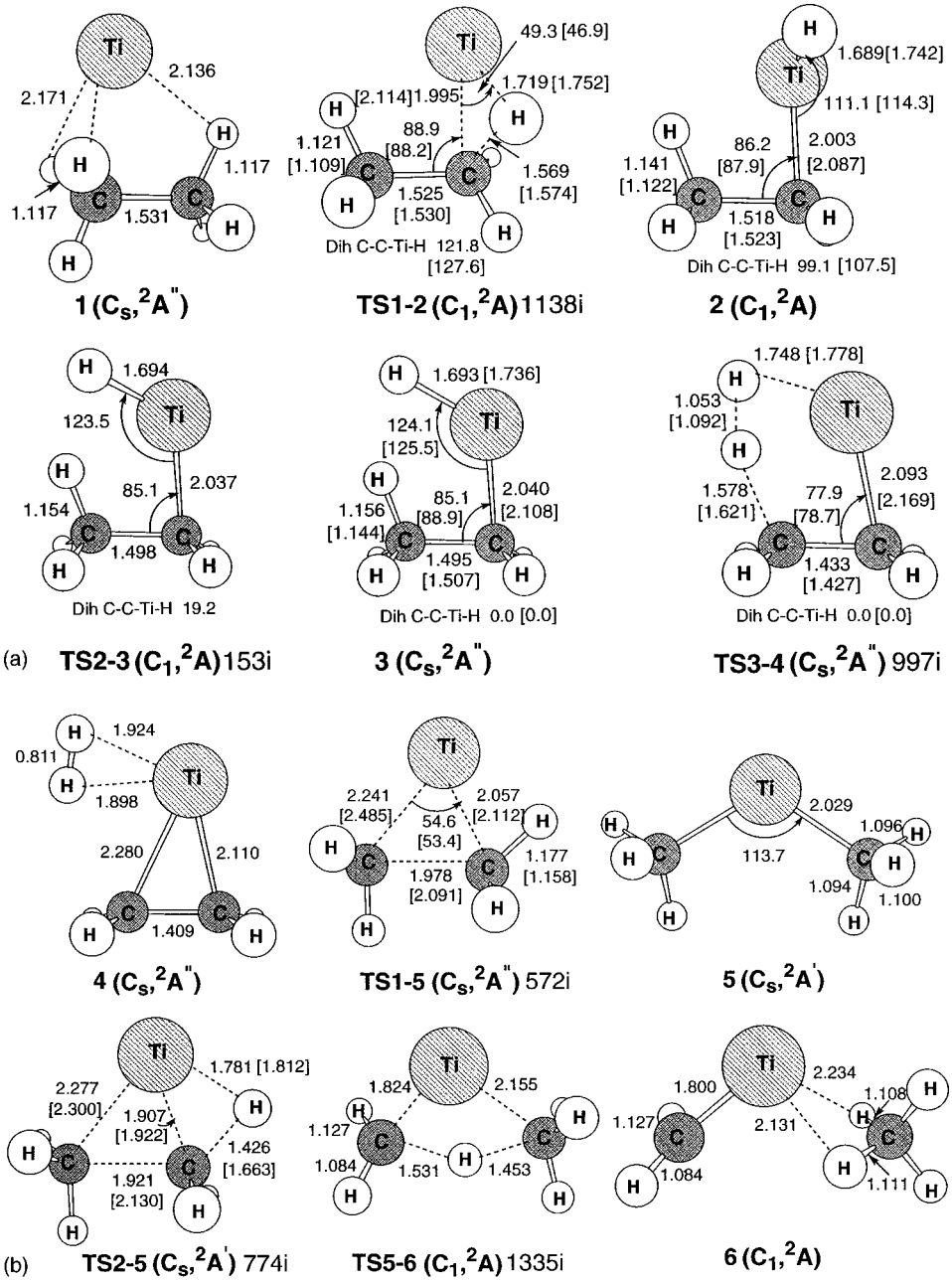

FIG. 3. Doublet structures for the reaction between Ti^+ and C_2H_6 (bond lengths in Å, bond angles in degrees); for TS's, the corresponding imaginary frequencies (cm^{-1}) are given. Values in brackets are CASSCF results.

at this level for the doublet **1** and **1a**. However, based on the results for the quartet surface, one may predict that the DFT doublet binding energies are also a few kcal/mol too large.

Starting from the $Ti^+\cdots C_2H_6$ complex, metal insertion into a C–H or C–C bond can be considered as the next reaction step. The C–H insertion described below starts from the complex **1**. The analogous C–H insertion starting from complex **1a** was also explored. Although the energy of the C–H insertion TS connecting complex **1a** with the corresponding $HTiC_2H_5^+$ product was 0.5 kcal/mol lower than the energy of the TS connecting complex **1**, the former TS leads to an energetically less favorable product, by ~10 kcal/mol at the B3LYP level. Therefore, the **1a** path was not pursued further.

The complete reaction paths for the H_2 and CH_4 eliminations will be discussed next. Figures 3 and 4 summarize all of the calculated structures for the doublet and quartet states, respectively. The energies relevant to the H_2 and CH_4 eliminations are collected in Tables II and III, and the corresponding energy profiles are depicted in Figs. 5 and 6, respectively. For each species the energy given is relative to the ground-state reactants $C_2H_6+Ti^+(^4F)$ and includes the ZPVE correction. The structure labels in Tables II and III and Figs. 5 and 6 correspond to those used in Figs. 3 and 4.

C. H_2 elimination path

The C–H insertion step in the H_2 elimination reaction involves breaking a C–H bond in **1** and forming the insertion product **2**, $HTiC_2H_5^+$ (oxidative addition), shown in Figs. 3 and 4. On the doublet surface, the B3LYP energy of **2** (C_1 symmetry) decreases by 4.8 kcal/mol relative to the complex **1**. This structure has a C–Ti distance of 2.003 Å (DFT) or 2.087 Å (CASSCF) and a nearly perpendicular C–C–Ti ar-

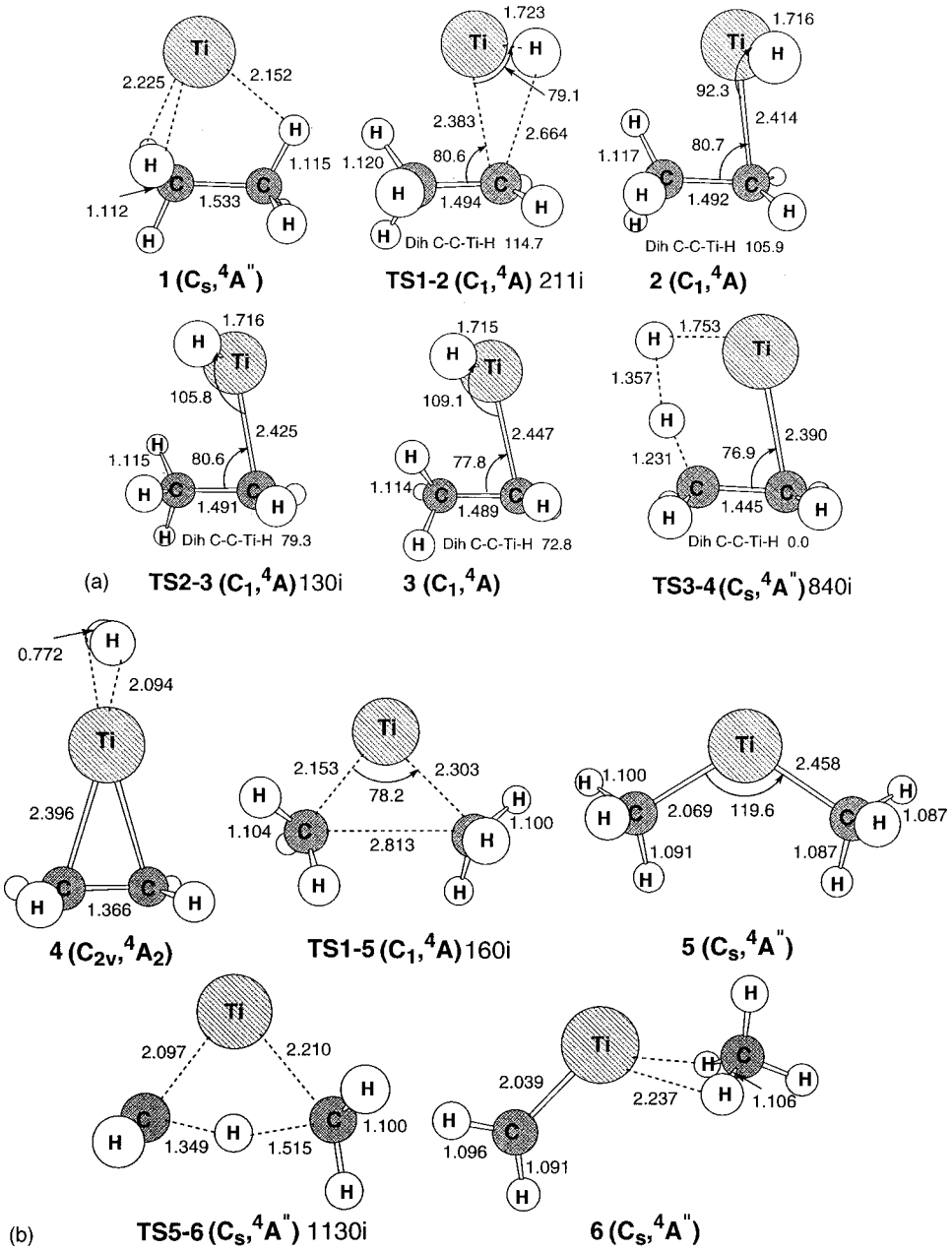

FIG. 4. Quartet structures for the reaction between Ti^+ and C_2H_6 (bond lengths in Å, bond angles in degrees); for TS's, the corresponding imaginary frequencies (cm^{-1}) are given.

rangement. The corresponding C–H insertion TS, **TS1-2**, is productlike, with a very similar C–Ti bond (Fig. 3). The B3LYP barrier height at this (adiabatic) doublet TS is 11.4 kcal/mol, relative to **1** (Table II). The net energy requirement relative to separated reactants is 5.2 kcal/mol. The corresponding CCSD(T) and MCQDPT2 barriers are 9.0 and 8.0 kcal/mol, respectively. In contrast, on the quartet surface, the energy of **2** increases with respect to **1** by 37.2, 37.7, 39.2 kcal/mol at the DFT, CCSD(T), and MCQDPT2 levels of theory, respectively (see below for explanation of this instability). Since the very late quartet C–H insertion **TS1-2** (Fig. 4) is even higher in energy [at DFT and CCSD(T)], a crossing occurs between the quartet and doublet surfaces in this region (cf. Fig. 5). This implies that the reaction will subsequently proceed on the doublet surface if the intersurface coupling interaction is sufficiently large. The crossing [Figs. 5(a), 5(c)] apparently precedes the doublet C–H insertion **TS1-2** which determines the adiabatic insertion barrier. This surface crossing will be discussed in more detail below.

In the next step on the doublet surface, the Ti–H bond in the C–H insertion product **2** rotates via **TS2-3** to the rotamer **3**, the latter having a planar structure ($^2A''$) with a slightly longer C–Ti bond than that in **2** (Fig. 3). All levels of theory agree that after accounting for the ZPVE correction, the rotation **TS2-3** becomes lower in energy than **3**, so that the rotamer may not correspond to a genuine minimum (Fig. 5), and the **TS2-3** may be irrelevant. Both DFT [Fig. 5(a)] and MCQDPT2 [Fig. 5(c)] find that **TS2-3** and **3** lie well below the $C_2H_6+Ti^+(^4F)$ reactants, whereas CCSD(T) locates the two species slightly above this asymptote. All methods predict **2** to be below the asymptote.

The relationship among **2**, **TS2-3**, and **3** is similar on the quartet surface. On this quartet surface (Fig. 5) all species

TABLE II. Relative energies for the H_2 elimination reaction (in kcal/mol).[a]

	DFT B3LYP	CCSD(T)	MCQDPT2
	$Ti^+ + C_2H_6 \rightarrow TiC_2H_4^+ + H_2$		
	Doublet		
$Ti^+ + C_2H_6$	14.3		13.6
$Ti^+ \cdots C_2H_6$ (**1**)	−6.2		1.2
C–H ins. TS (**TS1–2**)	5.2	9.0	8.0
$HTiC_2H_5^+$ (**2**)	−11.0	−1.7	−10.1
Ti–H rot. TS (**TS2–3**)	−6.9	1.9	−10.1
$HTiC_2H_5^+$ (**3**)	−6.8	2.1	−8.2
H_2 elim. TS (**TS3–4**)	1.5	9.5	−2.2
$TiC_2H_4^+ \cdots H_2$ (**4**)	−1.8	6.2	−3.6
$TiC_2H_4^+ + H_2$	0.6	7.5	−0.3
	Quartet		
$Ti^+ + C_2H_6$	0.0	0.0	0.0
$Ti^+ \cdots C_2H_6$ (**1**)	−20.1	−15.6	−18.8
C–H ins. TS (**TS1–2**)	17.3	23.1	17.0
$HTiC_2H_5^+$ (**2**)	17.1	22.1	20.4
Ti–H rot. TS (**TS2–3**)	17.1	21.6	
$HTiC_2H_5^+$ (**3**)	16.2	20.6	
H_2 elim. TS (**TS3–4**)	21.8	30.9	
$TiC_2H_4^+ \cdots H_2$ (**4**)	−6.8	3.1	−10.4
$TiC_2H_4^+ + H_2$	−1.2	7.7	2.8

[a]All energies are relative to the $Ti^+(^4F) + C_2H_6$ ground-state reactants and include the ZPVE corrections.

TABLE III. Relative energies for the CH_4 elimination reaction (in kcal/mol).[a]

	DFT B3LYP	CCSD(T)
	$Ti^+ + C_2H_6 \rightarrow TiCH_2^+ + CH_4$	
	Doublet	
$Ti^+ + C_2H_6$	14.3	
$Ti^+ \cdots C_2H_6$ (**1**)	−6.2	
C–H ins. TS (**TS1–2**)	5.2	9.0
$HTiC_2H_5^+$ (**2**)	−11.0	−1.7
C–C ins. TS (**TS2–5**)	16.7	25.0
$Ti(CH_3)_2^+$ (**5**)	−22.1	−11.6
1,3 H shift TS (**TS5–6**)	8.1	15.1
$TiCH_2^+ \cdots CH_4$ (**6**)	−3.4	1.9
$TiCH_2^+ + CH_4$	11.0	17.0
	Quartet	
$Ti^+ + C_2H_6$	0.0	0.0
$Ti^+ \cdots C_2H_6$ (**1**)	−20.1	−15.6
$Ti(CH_3)_2^+$ (**5**)	11.0	18.3
1,3 H shift TS (**TS5–6**)	26.9	36.0
$TiCH_2^+ \cdots CH_4$ (**6**)	6.0	12.7
$TiCH_2^+ + CH_4$	19.4	25.6

[a]All energies are relative to the $Ti^+(^4F) + C_2H_6$ ground-state reactants and include the ZPVE corrections.

between **1** and **3** lie well above the $C_2H_6 + Ti^+(^4F)$ asymptote. Unlike the doublet, the quartet Ti^+ apparently cannot form stable insertion products. For instance, after forming an H–Ti bond in the quartet structure **2**, by singlet coupling a pair of electrons, the missing spin contribution is ''borrowed'' from the neighboring C atom to conserve the quartet character. This is confirmed by the calculated spin density distribution in the quartet **2** of ~2.2 and 0.8 on the Ti and neighboring C atoms, respectively. The quartet structures show correspondingly much weaker C–Ti bonds with the distances longer by ~0.4 Å as compared to the doublet counterparts (cf. Figs. 3 and 4).

In the next step on the doublet surface, the $HTiC_2H_5^+$ rotamer **3** can undergo reductive elimination via the planar H_2 elimination **TS3-4** to form the molecular complex $TiC_2H_4^+ \cdots H_2$(**4**) (Fig. 3). For **TS3-4**, both DFT and CASSCF predict a C–C–Ti angle of ~80°. The C_s intermediate **4** ($^2A''$), obtained by following the IRC from **TS3-4**, has the H_2 unit rotated in the C–C–Ti symmetry plane. Also, it exhibits asymmetrically lengthened Ti–C bonds and a shortened C–C bond relative to the $TiC_2H_4^+(^2A_1)$ product. These structural changes indicate a weaker Ti^+–C_2H_4 interaction in the molecular complex **4**, as compared to the final $TiC_2H_4^+(^2A_1)$ product on this path. The DFT C_{2v} $TiC_2H_4^+ \cdots H_2$ structure with the H_2 unit *perpendicular* to the C–C–Ti plane is 1.4 kcal/mol higher in energy and has two imaginary frequencies.

For the reductive elimination step B3LYP predicts a barrier of 1.5 kcal/mol above the $C_2H_6 + Ti^+(^4F)$ reactants with the resulting complex **4** located 1.8 kcal/mol below this asymptote [Fig. 5(a)]. According to CCSD(T), Fig. 5(b), the reductive elimination step must conquer a higher barrier of 9.5 kcal/mol above $C_2H_6 + Ti^+(^4F)$ [comparable to the CCSD(T) C–H insertion barrier], and the complex **4** is located 6.2 kcal/mol above this asymptote (Fig. 5). The MCQDPT2 surface is more similar to the DFT result, since it predicts that all points after the insertion step **TS1-2** are below the asymptote.

On the quartet surface, the complex $TiC_2H_4^+ \cdots H_2$ **4** is very stable, well below the asymptote according to both DFT and MCQDPT2. The quartet **4** has C_{2v} symmetry ($^4A_2$) with the H_2 unit perpendicular to the C–C–Ti plane (Fig. 4).[35] Since the C–Ti and C–C distances in quartet **4** and the $TiC_2H_4^+(^4B_1)$ product (Fig. 1) are nearly the same, the Ti^+–C_2H_4 interaction in **4** is similar to that in $TiC_2H_4^+(^4B_1)$, in contrast to the doublet case discussed above. Indeed, all levels of theory predict that the molecular complex **4** in the quartet state is lower in energy than its doublet counterpart. As a result, another spin crossing occurs in this region and the H_2 elimination proceeds back to the original (quartet) surface (Fig. 5).

In the final step the H_2 molecule is eliminated, yielding the $TiC_2H_4^+$ product. According to DFT, the latter is left in the quartet state at a net cost of 5.2 kcal/mol, and the overall H_2 elimination reaction starting with the $C_2H_6 + Ti^+(^4F)$ reactants is slightly exothermic, by 1.2 kcal/mol [Fig. 5(a)]. The CCSD(T) calculations predict that $TiC_2H_4^+$ is left in the doublet state and the overall H_2 elimination reaction is slightly endothermic, by 7.5 kcal/mol [Fig. 5(b)]. The MCQDPT2 calculations are in qualitative agreement with CCSD(T), since this method predicts a doublet final product with a net cost less than 8.0 kcal/mol and essentially a thermoneutral reaction. All three levels of theory predict the final doublet and quartet products to be very similar in energy.

D. CH_4 elimination path

There are indirect and direct C–C insertion mechanisms leading to CH_4 from the complex **1**. For the indirect mechanism, on the doublet surface, the C–H insertion step is com-

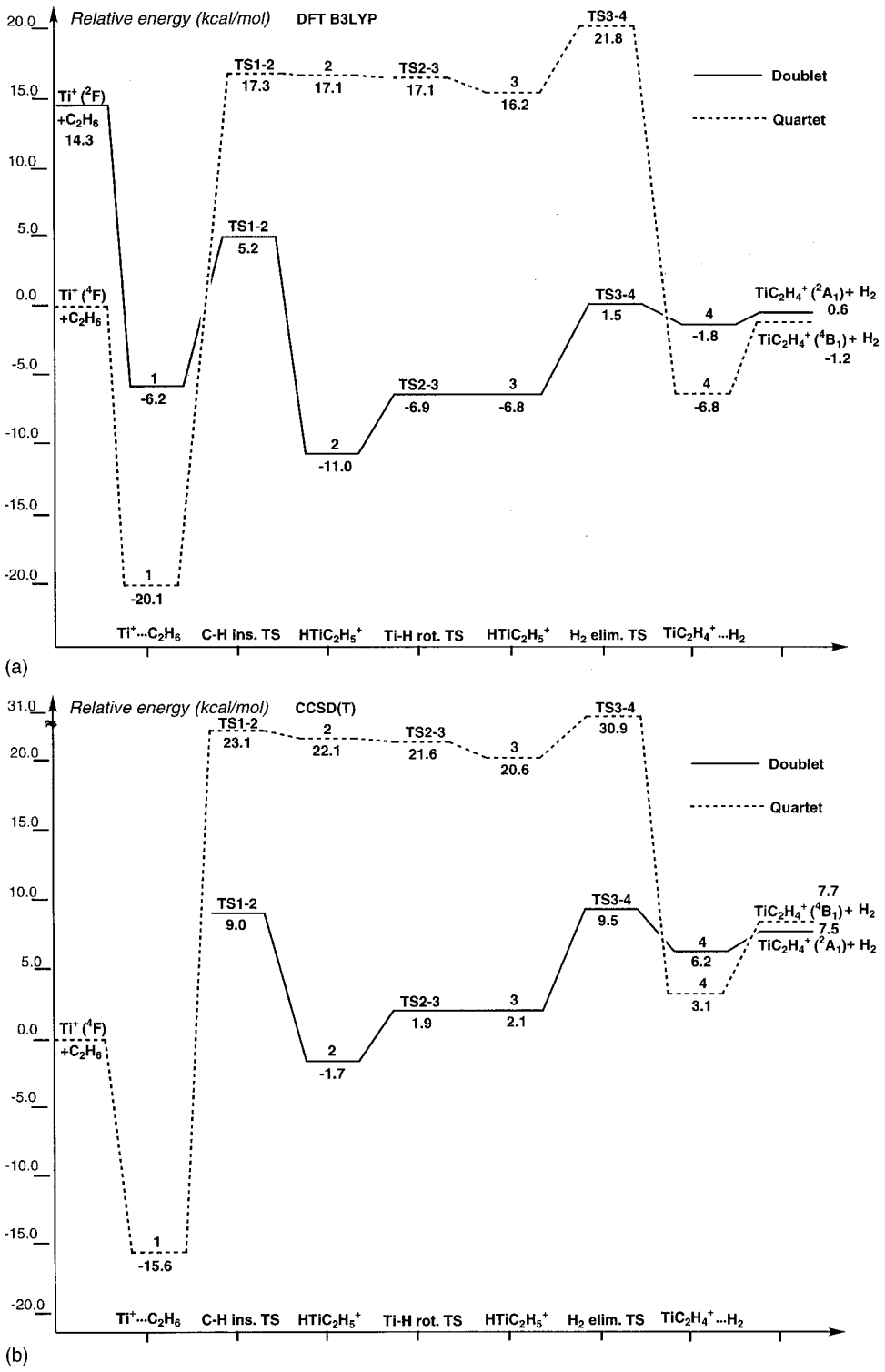

FIG. 5. The energy profiles for the $Ti^+ + C_2H_6 \rightarrow TiC_2H_4^+ + H_2$ reaction calculated at the (a) DFT B3LYP, (b) CCSD(T), and (c) MCQDPT2 level.

mon for H_2 and CH_4 elimination paths (Fig. 6). In the next step on that surface, the $HTiC_2H_5^+$ intermediate **2** can be transformed to the $Ti(CH_3)_2^+$ dimethyl cation **5** via the four-center **TS2-5** (Fig. 3). The latter TS leads from the C–H insertion product to the C–C insertion product and features partially broken C–C and C–H bonds. The optimal structure of $Ti(CH_3)_2^+$ **5** is bent and has C_s symmetry ($^2A'$) with the two methyls eclipsed and the two in-plane hydrogens nearer each other than the four out-of-plane hydrogens (Fig. 3). A DFT C_{2v} structure with the same orientation of the methyls was found to be 0.04 kcal/mol higher in energy and showed a small imaginary frequency with the eigenvector indicating rotation of both methyls in the same direction. The DFT (CCSD(T)) indirect C–C insertion barrier via **TS2-5** is 16.7 (25.0) kcal/mol above the $C_2H_6+Ti^+(^4F)$ reactants. B3LYP predicts **5** to be the global minimum on the reaction path, whereas CCSD(T) predicts the initial complex to be the global minimum. Despite a very careful search, a quartet indirect C–C insertion TS was not located.

A direct C–C insertion TS from complex **1** to the dim-

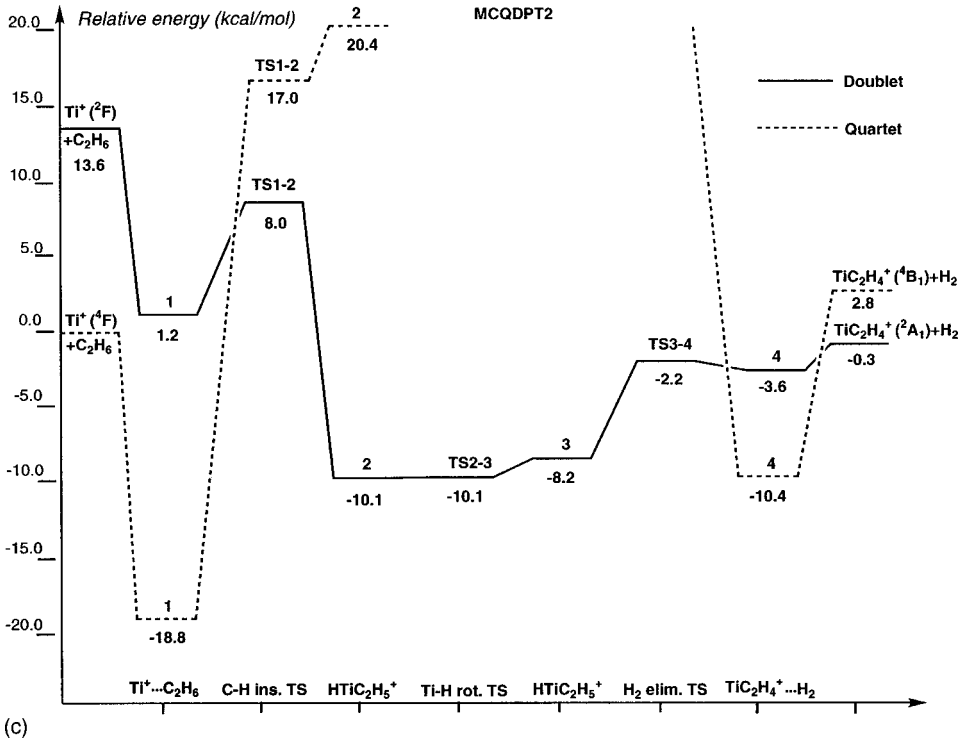

FIG. 5. (*Continued.*)

ethyl species **5** was found for both spin states and is denoted **TS1-5** in Figs. 3 and 4. Because the doublet DFT **TS1-5** has significant spin contamination, its CASSCF counterpart (Fig. 3) was also located. On the doublet surface, the actual C–C insertion barrier relative to the initial reactants via **TS1-5** (not shown in Table III) is found to be somewhat higher than that for the indirect mechanism, i.e., being 20.0 [Fig. 6(a)] and 27.9 kcal/mol at the DFT B3LYP and MCQDPT2 levels, respectively [note that the CCSD(T) barrier for the direct C–C insertion is not shown in Fig. 6(b); this part of the surface was evaluated using MCQDPT2].

Insertion of quartet Ti^+ into the C–C bond is not thermodynamically favorable as discussed earlier for the C–H insertion. The dimethyl species **5** on the quartet surface is 31 and 34 kcal/mol above complex **1** at the DFT and CCSD(T) levels, respectively. As a result, a surface crossing occurs (cf. Fig. 6). Assuming significant spin-orbit coupling, the reaction moves to the doublet surface and returns there after passing the quartet direct C–C insertion **TS1-5**.

The next step on the doublet surface is 1,3 hydrogen migration from **5** via **TS5-6**, leading to the molecular complex $TiCH_2^+\cdots CH_4$(**6**) (Fig. 3). The complex **6** is 3.4 kcal/mol below and 1.9 kcal/mol above $C_2H_6+Ti^+(^4F)$ with DFT and CCSD(T), respectively. **TS5-6** is located at 8.1 and 15.1 kcal/mol at these same levels of theory. Complex **6** involves η^2 coordinated CH_4 and was obtained by following the IRC from **TS5-6**. The ''asymmetric'' $TiCH_2^+$ product already formed within **6** can be easily recognized [cf. Figs. 1(c) and 3]. A DFT C_s symmetry η^3 coordinated structure of $TiCH_2^+\cdots CH_4$ was also found, but it is ~3 kcal/mol less stable and has one imaginary frequency with the eigenvector showing distortion to C_1. The final step for this mechanism is release of a CH_4 molecule at the cost of 14.4 kcal/mol (DFT) and 15.1 kcal/mol [CCSD(T)]. The overall CH_4 elimination reaction starting with the $C_2H_6+Ti^+(^4F)$ reactants is endothermic by 11.0, 17.0, and 7.2 kcal/mol at the DFT B3LYP, CCSD(T), and MCQDPT2 levels of theory, respectively.

At thermal energies after passing **TS1-5**, the quartet surface is not involved in the CH_4 elimination reaction. However, this path and the relevant structures are included in Table III and Fig. 6 for comparison purposes. The quartet complex **6** is 9.4 (DFT) or 10.8 kcal/mol [CCSD(T)] less stable than the doublet analog, which corresponds roughly to the doublet-quartet splitting for the $TiCH_2^+$ product discussed above. Note that the quartet $Ti(CH_3)_2^+$ species **5** exhibits a reduced symmetry as shown by the inequivalent Ti–C bonds (Fig. 4).[36]

E. Spin-orbit coupling

Three approaches were described in Sec. II for assessing the behavior in the doublet-quartet crossing region. These three methods are illustrated in Figs. 7–9 for the region between **1** and **TS1-2**. The spin-orbit coupling constant (SOCC), defined as the square root of the sum of squares of the absolute values of H_{so} matrix elements, is found to be in the range 50–55 cm^{-1} for all three methods.

Figure 10 shows the energies split due to the spin-orbit interaction. The numbers in parentheses give the degeneracies of the energy levels. The value of $C=52.5\,cm^{-1}$ was normalized by the level degeneracy according to $C^2/(2S+1)$, $S=1/2$, and used for the square of the diabatic potential to estimate the Landau–Zener transition probability.[37,38] The probability is plotted in Fig. 11. The value at room temperature is 13.4%.

The value of the spin-orbit coupling constant is smaller than might be expected for a compound containing an atom

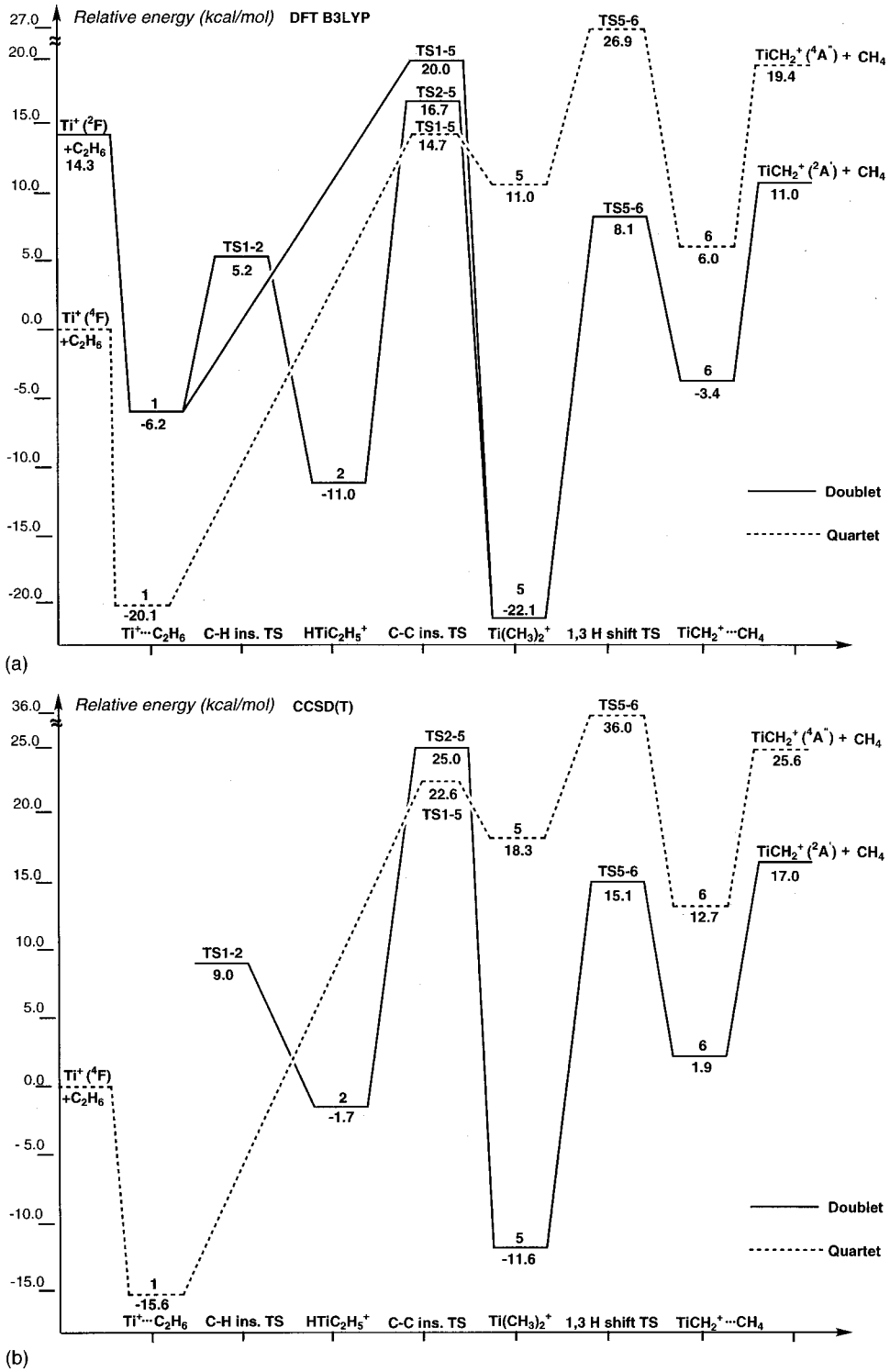

FIG. 6. The energy profiles for the $Ti^+ + C_2H_6 \rightarrow TiCH_2^+ + CH_4$ reaction calculated at the (a) DFT B3LYP and (b) CCSD(T) level. Note that the section of the surface connecting structure **1** with **5** in part (b) was obtained with MCQDPT2, not CCSD(T), due to the large configurational mixing in this region.

as heavy as titanium; however, it is large enough to alter the course of the otherwise energy forbidden reaction (at room temperature) to allow a channel of the quartet state of the reactants to proceed to the energetically accessible doublet surface. Interestingly, another two potential energy crossings appear to occur near the products (Fig. 5). However, they do not appear to affect the dynamics to a significant extent due to small energy differences of the two surfaces in those regions. For this reason, these regions were not explored further.

IV. CONCLUSIONS

(i) The $Ti^+ + C_2H_6 \rightarrow TiC_2H_4^+ + H_2$ and $Ti^+ + C_2H_6 \rightarrow TiCH_2^+ + CH_4$ elimination reactions are initiated with the formation of the η^3 coordinated $Ti^+ \cdots C_2H_6$ ion-induced dipole complex in the quartet state. Due to instability of the quartet C–H and C–C insertion products relative to the doublet counterparts, a spin crossing occurs and the two reactions proceed on the low-spin surface.

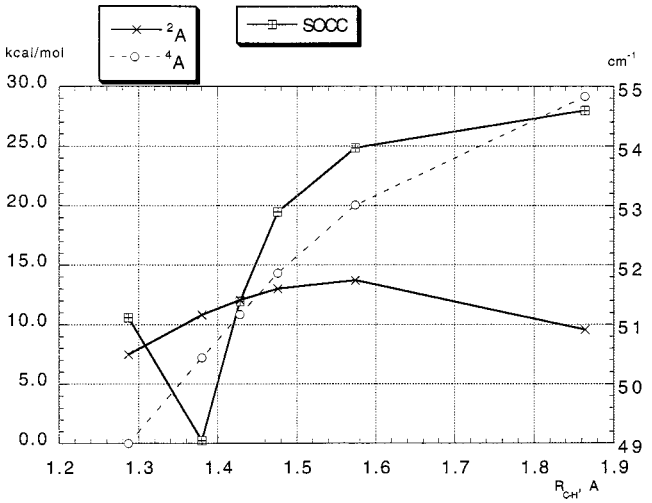

FIG. 7. Energy and spin-orbit coupling constant (SOCC) along the doublet IRC from **TS1-2** in the direction of complex **1**.

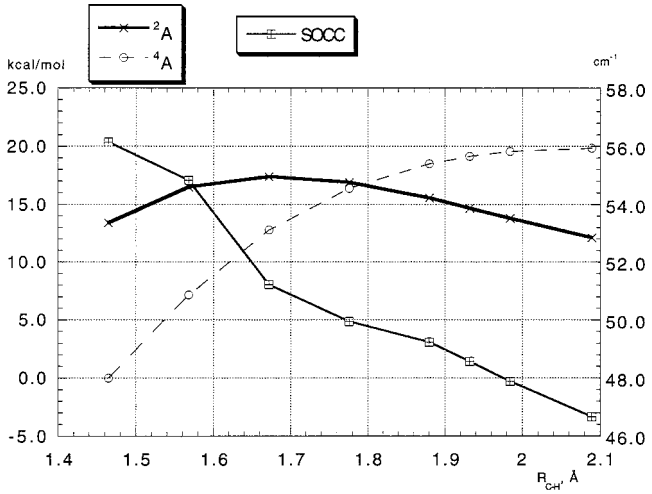

FIG. 8. Energy and SOCC along the quartet IRC from **TS1-2** in the direction of complex **1**.

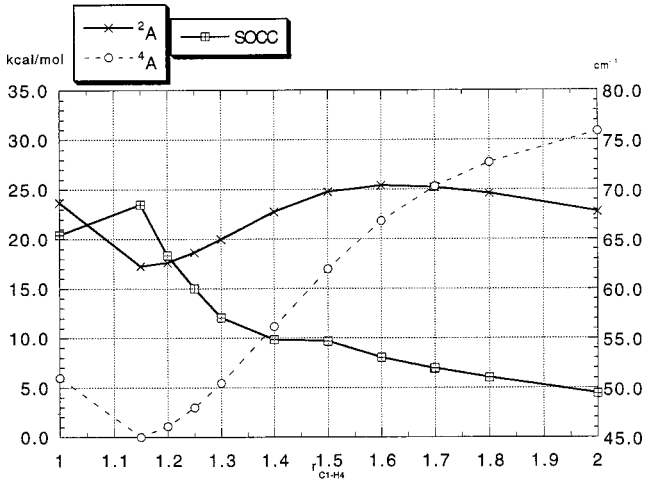

FIG. 9. Energy and SOCC along the averaged IRC from **TS1-2** in the direction of complex **1**.

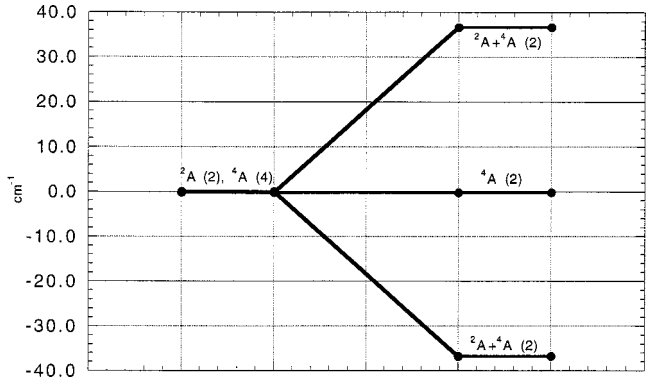

FIG. 10. Energy levels at the crossing (along the averaged IRC), rC–H $=1.698$ Å.

(ii) The overall H_2 elimination reaction is calculated to be slightly exothermic by DFT B3LYP and MCQDPT2, and slightly endothermic by CCSD(T). The C–H insertion TS (DFT B3LYP and MCQDPT2) or C–H insertion TS and H_2 elimination TS [CCSD(T)] are the highest energy points en route to the products, with a net energy requirement of 5–9 kcal/mol, depending on the level of theory. In comparison, for the Co^+- and Fe^+-mediated elimination of H_2 from C_2H_6 studied recently with DFT,[39] the C–H insertion TS was located below the entrance channel and the H_2 loss TS was the rate determining step. The higher relative energy of the C–H insertion TS in the Ti^+ case might result from the more shallow potential well of its initial complex as compared to the Co^+ and Fe^+ analogs. The actual depth of this well determines whether insertion barriers lie below or above the entrance channel.[40] Finally, consistent with the labeling experiments,[4] the results presented here suggest the 1,2 H_2 elimination mechanism is most likely.

(iii) The overall CH_4 elimination reaction is predicted to be endothermic, by 11.0 and 17.0 and 7.2 kcal/mol at the DFT B3LYP, CCSD(T) and MCQDPT2 levels of theory, respectively. Although the C–C insertion product, $Ti(CH_3)_2^+$, is a low energy intermediate, a high C–C insertion barrier prevents observation of this species under thermal conditions. Based on the

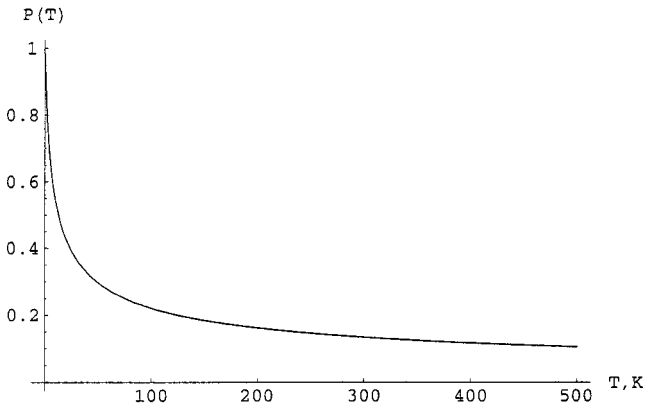

FIG. 11. Transition probability at the doublet/quartet crossing.

calculated energy profiles it is suggested that the initial complex $Ti^+\cdots C_2H_6$ in the quartet state is a likely candidate for the adduct ion stabilized in the flow tube experiments.[3,6]

(iv) With the possible exception of transition state structures, DFT/B3LYP appears to be a viable and efficient method for predicting structures for stationary points on potential energy surfaces for reactions such as those studied here. A reliable procedure for studying such potential energy surfaces therefore appears to be a combination of B3LYP geometry predictions followed by an analysis of the energetics using either multireference perturbation theory or CCSD(T). The main drawback of the latter method is the difficulty of treating phenomena near surface crossings, since there two (or more) electronic states are involved. Convergence of the coupled-cluster equations also appears to be problematic in these regions.

ACKNOWLEDGMENTS

This work was supported in part by the Department of Energy Basic Energy Sciences Division via the Ames Laboratory (support of D.F.) and the Air Force Office of Scientific Research (support of J.M.). The calculations were performed on computers made available by the Department of Energy and by a Shared University Research grant from IBM.

[1] (a) P. A. M. van Koppen, P. R. Kemper, and M. T. Bowers, in *Organometallic Ion Chemistry*, edited by B. S. Freiser (Kluwer, Dordrecht, The Netherlands, 1996), p. 157; (b) P. B. Armentrout, in *Gas-Phase Inorganic Chemistry*, edited by D. H. Russell (Plenum, New York, 1989), p 1; (c) in *Selective Hydrocarbon Activation: Principles and Progress*, edited by J. A. Davies, P. L. Watson, J. Liebman and A. Greenberg (VCH, New York, 1990), p. 467; (d) J. C. Weisshaar, in *Advances in Chemical Physics*, edited by C. Ng (Wiley Interscience, New York, 1992), Vol. 82, pp. 213–261.

[2] G. D. Byrd, R. C. Burnier, and B. S. Freiser, J. Am. Chem. Soc. **104**, 3565 (1982).

[3] (a) R. Tonkyn and J. C. Weisshaar, J. Phys. Chem. **90**, 2305 (1986); (b) **92**, 92 (1988).

[4] M. A. Tolbert and J. L. Beauchamp, J. Am. Chem. Soc. **108**, 7509 (1986).

[5] L. S. Sunderlin and P. B. Armentrout, Int. J. Mass Spectrom. Ion Processes **94**, 149 (1989).

[6] R. S. MacTaylor, W. D. Vann, and A. W. Castleman, Jr., J. Phys. Chem. **100**, 5329 (1996).

[7] R. G. Parr and W. Yang, *Density Functional Theory of Atoms and Molecules* (Oxford University Press, Oxford, 1989).

[8] *Density Functional Methods in Chemistry*, edited by J. K. Labanowski and J. W. Andzelm (Springer, Berlin, 1991).

[9] A. D. Becke, Phys. Rev. A **38**, 3098 (1988).

[10] (a) A. D. Becke, J. Chem. Phys. **98**, 1372 (1993); (b) **98**, 5648 (1993).

[11] P. J. Stevens, F. J. Devlin, C. F. Chabalowski, and M. J. Frisch, J. Phys. Chem. **98**, 11623 (1994).

[12] C. Lee, W. Yang, and R. G. Parr, Phys. Rev. B **37**, 785 (1988).

[13] S. H. Vosko, L. Wilk, and M. Nusair, Can. J. Phys. **58**, 1200 (1980).

[14] (a) K. Fukui, Acc. Chem. Res. **14**, 363 (1981); (b) K. Ishida, K. Morokuma, and A. Komornicki, J. Chem. Phys. **66**, 2153 (1977); (c) M. W. Schmidt, M. S. Gordon, and M. Dupuis, J. Am. Chem. Soc. **107**, 2585 (1985); (d) B. C. Garrett, M. J. Redmon, R. Steckler, D. G. Truhlar, K. K. Baldridge, D. Bartol, M. W. Schmidt, and M. S. Gordon, J. Chem. Phys. **92**, 1476 (1988); (e) K. K. Baldridge, M. S. Gordon, R. Steckler, and D. G. Truhlar, *ibid.* **93**, 5107 (1989).

[15] (a) C. Gonzalez and H. B. Schlegel, J. Chem. Phys. **90**, 2154 (1989); (b) C. Gonzalez and H. B. Schlegel, J. Phys. Chem. **94**, 5523 (1990).

[16] A. J. H. Wachters, J. Chem. Phys. **52**, 1033 (1970).

[17] A. K. Rappé, T. A. Smedley, and W. A. Goddard III, J. Phys. Chem. **85**, 2607 (1981).

[18] The standard modifications implemented in the GAMESS code (Ref. 26) the resulting basis set is stored as TZV.

[19] (a) T. H. Dunning, J. Chem. Phys. **55**, 716 (1971); (b) S. Huzinaga, *ibid.* **42**, 1293 (1965).

[20] (a) M. J. Frisch, G. W. Trucks, H. B. Schlegel, P. M. W. Gill, B. G. Johnson, M. A. Robb, J. R. Cheeseman, T. A. Keith, G. A. Petersson, J. A. Montgomery, K. Raghavachari, M. A. Al-Laham, V. G. Zakrzewski, J. V. Ortiz, J. B. Foresman, J. Cioslowski, B. B. Stefanov, A. Nanayakkara, M. Challacombe, C. Y. Peng, P. Y. Ayala, W. Chen, M. W. Wong, J. L. Andres, E. S. Replogle, R. Gomperts, R. L. Martin, D. J. Fox, J. S. Binkley, D. J. Defrees, J. Baker, J. P. Stewart, M. Head-Gordon, C. Gonzalez, and J. A. Pople, GAUSSIAN 94, Gaussian, Inc., Pittsburgh, PA, 1995; (b) M. J. Frisch, G. W. Trucks, M. Head-Gordon, P. M. W. Gill, M. W. Wong, J. B. Foresman, B. G. Johnson, H. B. Schlegel, M. A. Robb, E. S. Replogle, R. Gomperts, J. L. Andres, K. Raghavachari, J. S. Binkley, C. Gonzalez, R. L. Martin, D. J. Fox, D. J. DeFrees, J. Baker, J. J. P. Stewart, and J. A. Pople, GAUSSIAN 92 DFT, Gaussian, Inc., Pittsburgh, PA, 1993. ''INT=FineGrid'' option was used throughout.

[21] (a) J. Cizek, Adv. Chem. Phys. **14**, 35 (1969); (b) G. D. Purvis, R. J. Bartlett, J. Chem. Phys. **76**, 1910 (1982); (c) G. E. Scuseria, C. L. Janssen, H. F. Schaefer, III, *ibid.* **89**, 7382 (1988); (d) K. Raghavachari, G. W. Trucks, J. A. Pople, and M. Head-Gordon, Chem. Phys. Lett. **157**, 479 (1989); (e) G. E. Scuseria and H. F. Schaefer III, J. Chem. Phys. **90**, 3700 (1989); (f) J. D. Watts, J. Gauss, and R. J. Bartlett, *ibid.* **98**, 8718 (1993); (g) J. A. Pople, M. Head-Gordon, and K. Raghavachari, *ibid.* **87**, 5968 (1987).

[22] (a) K. Raghavachari and G. W. Trucks, J. Chem. Phys. **91**, 1062 (1989); (b) P. J. Hay, *ibid.* **66**, 4377 (1977); (c) The final Ti basis of the form $(15s11p6d2f)/[10s7p4d2f]$ was used in conjunction with the standard Pople's $6-311+G(2d,2p)$ basis sets for C and H atoms. For the latter basis, see M. J. Frisch, J. A. Pople, and J. S. Binkley, *ibid.* **80**, 3265 (1984).

[23] For a review of the CASSCF method, see B. O. Roos, in *Ab Initio Methods in Quantum Chemistry—II*, edited by K. P. Lawley (Wiley, Chichester, U.K., 1987), pp. 399–445. The *f* function exponents and coefficients were obtained from the Extensible Computational Chemistry Environment Basis Set Database, Version 1.0, as developed and distributed by the Molecular Science Computing Facility, Environmental and Molecular Sciences Laboratory, which is part of the Pacific Northwest Laboratory.

[24] (a) H. Nakano, J. Chem. Phys. **99**, 7983 (1993); (b) H. Nakano, Chem. Phys. Lett. **207**, 372 (1993).

[25] H. A. Bethe and E. E. Salpeter, *Quantum Mechanics of the One and Two Electron Atoms* (Plenum, New York, 1977).

[26] GAMESS (General Atomic and Molecular Electronic Structure System), M. W. Schmidt, K. K. Baldridge, J. A. Boatz, S. T. Elbert, M. S. Gordon, J. H. Jensen, S. Koseki, N. Matsunaga, K. A. Nguyen, S. Su, T. L. Windus, M. Dupuis, and J. A. Montgomery, Jr., J. Comput. Chem. **14**, 1347 (1993).

[27] J. Sugar and C. Corioliss, J. Phys. Chem. Ref. Data **14**, Suppl. No 2. (1985).

[28] A recent review article comparing performance of the DFT B3LYP approach against the traditional *ab initio* methods for transition metal systems can be mentioned here: P. E. M. Siegbahn, in *Advances in Chemical Physics*, edited by I. Prigogine and S. A. Rice (Wiley, New York, 1996), Vol. XCIII, pp. 333–386.

[29] W. J. Hehre, L. Radom, P. v. R. Schleyer, and J. A. Pople, *Ab Initio Molecular Orbital Theory* (Wiley, New York, 1986).

[30] J. Andzelm, Pol. J. Chem. **72**, 1747 (1998). Supplement in honor of Wlodzimierz Kolos.

[31] M. Sodupe, C. W. Bauschlicher, S. R. Langhoff, and H. Partridge, J. Phys. Chem. **96**, 2118 (1992). Note that the state referred to as $^4B_1$ in the present work is denoted $^4B_2$ by Sodupe *et al.*

[32] Note that the TZVP+*f* basis set was used for the CASSCF geometry optimization of $TiC_2H_4^+$ to describe better the Ti^+–C_2H_4 interaction.

[33] (a) A. Ricca and C. W. Bauschlicher, Chem. Phys. Lett. **245**, 150 (1995); (b) M. C. Holthausen, M. Mohr, and W. Koch, *ibid.* **240**, 245 (1995); (c) C. W. Bauschlicher, H. Partridge, J. A. Sheehy, S. R. Langhoff, and M. Rosi, J. Phys. Chem. **96**, 6969 (1992).

[34] We did not find a stationary point corresponding to the η^1C–H coordination.
[35] The C_{2v} structure with the perpendicular H_2 unit and corresponding to the $^4A_1$ state was 0.6 kcal/mol higher in energy and showed a small imaginary frequency.
[36] This is related to the corresponding spin density distribution of ~2.2 and 0.8 on the Ti and C atoms, the latter atom connected to Ti with the longer bond of 2.46 Å. The symmetry breaking related to the insufficient correlation level for the Co analog, $Co(CH_3)_{2^+}$, was reported by Perry *et al.*, J. K. Perry, W. A. Goddard III, and G. Ohanessian, J. Chem. Phys. **97**, 7560 (1992).
[37] H. Nakamura, J. Chem. Phys. **87**, 4031 (1987).
[38] D. G. Fedorov and M. S. Gordon, J. Chem. Phys. **112**, 5611 (2000).
[39] (a) M. C. Holthausen, A. Fiedler, H. Schwarz, and W. Koch, J. Phys. Chem. **100**, 6236 (1996); (b) M. C. Holthausen and W. Koch, J. Am. Chem. Soc. **118**, 9932 (1996).
[40] J. K. Perry, G. Ohanessian, W. A. Goddard III, J. Phys. Chem. **97**, 5238 (1993).